*Stem Cells Translational Medicine*, 2022, **11**, 876–888
https://doi.org/10.1093/stcltm/szac042
Advance access publication 27 June 2022
**Original Research**

# Acetabular Reaming Is a Reliable Model to Produce and Characterize Periarticular Heterotopic Ossification of the Hip

**Stefano Negri[1,2,‡], Yiyun Wang[1,‡], Zhao Li[1], Qizhi Qin[1], Seungyong Lee[1], Masnsen Cherief[1], Jiajia Xu[1], Ginny Ching-Yun Hsu[1], Robert Joel Tower[3], Bradley Presson[2], Adam Levin[4], Edward McCarthy[1], Benjamin Levi[3], Aaron W. James[*,1]**

[1]Department of Pathology, Johns Hopkins University, Baltimore, MD, USA
[2]Orthopaedic and Trauma Surgery Unit, Department of Surgery, Dentistry, Paediatrics and Gynaecology of the University of Verona, Verona, Italy
[3]Center for Organogenesis Research and Trauma, University of Texas Southwestern, Dallas, TX, USA
[4]Department of Orthopaedics, Johns Hopkins University, Baltimore, MD, USA

*Corresponding author: Aaron W. James, 720 Rutland Avenue, Room 524A, Baltimore, MD 21205, USA. Tel: +1 410 502 4143; Fax: +1 410 955 9777; Email: awjames@jhmi.edu
‡Contributed equally.

## Abstract

Heterotopic ossification (HO) is a pathologic process characterized by the formation of bone tissue in extraskeletal locations. The hip is a common location of HO, especially as a complication of arthroplasty. Here, we devise a first-of-its-kind mouse model of post-surgical hip HO and validate expected cell sources of HO using several HO progenitor cell reporter lines. To induce HO, an anterolateral surgical approach to the hip was used, followed by disclocation and acetabular reaming. Animals were analyzed with high-resolution roentgenograms and micro-computed tomography, conventional histology, immunohistochemistry, and assessments of fluorescent reporter activity. All the treated animals' developed periarticular HO with an anatomical distribution similar to human patients after arthroplasty. Heterotopic bone was found in periosteal, inter/intramuscular, and intracapsular locations. Further, the use of either PDGFRα or scleraxis (Scx) reporter mice demonstrated that both cell types gave rise to periarticular HO in this model. In summary, acetabular reaming reproducibly induces periarticular HO in the mouse reproducing human disease, and with defined mesenchymal cellular contributors similar to other experimental HO models. This protocol may be used in the future for further detailing of the cellular and molecular mediators of post-surgical HO, as well as the screening of new therapies.

**Key words:** heterotopic bone; hip arthroplasty; myositis ossificans; PDGFRα; scleraxis.

Received: 18 November 2021; Accepted: 7 May 2022.

**Graphical Abstract**

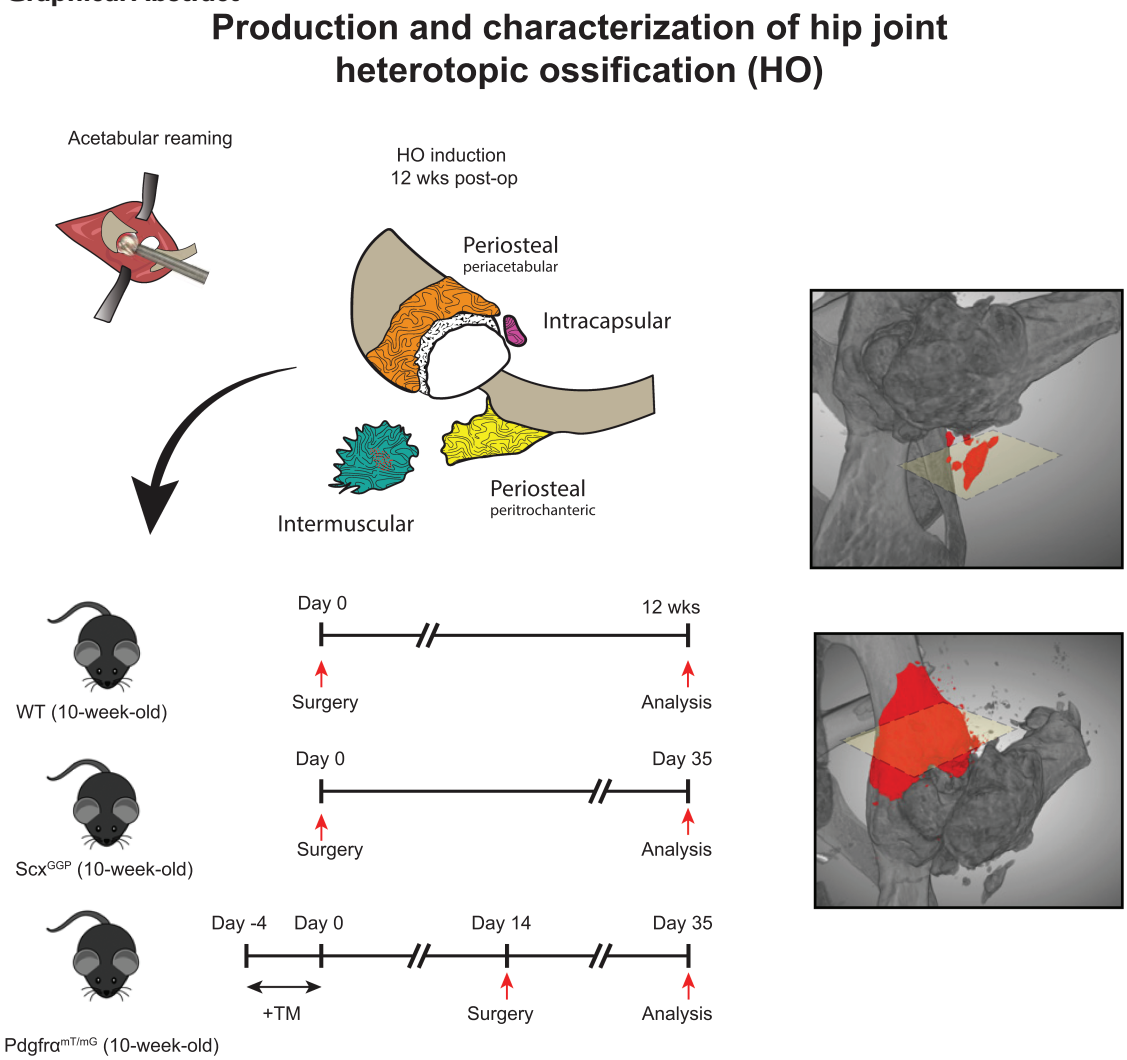


Heterotopic ossification (HO) of the hip was induced using an acetabular reaming model. Heterotopic bone was found in periosteal, inter/intramuscular, and intracapsular locations. Further, the use of either PDGFRα or Scleraxis (Scx) reporter mice demonstrated that both cell types gave rise to a portion of osteochondral cells in periarticular HO.

## Significance Statement

Although periarticular HO after hip arthroplasty is common, no mouse models have been developed. Our study represents the first mouse model for the study of HO of the hip, which could be leveraged for the further examination of cellular contributions to HO, use of transgenic mouse models to decipher molecular mechanisms of post-surgical HO, and the screening of new therapies for this common and potentially disabling condition.

## Introduction

Heterotopic ossification (HO) is a process that involves the formation of bone in extra-skeletal locations such as muscle and soft tissue.[1] In its most severe manifestations, this pathological bone tissue growth can result in excruciating pain and a lack of range of motion (ROM)[2]. Despite the fact that HO can form in a variety of anatomic sites such as tendons, ligaments, and muscles, it is always derived from tissue-resident connective tissue mesenchymal progenitor cells.[2-6] Here, predominantly local stromal/ fibroblastic cells of mesenchymal origin within connective tissue[3,6-9] undergo abnormal osteochondral differentiation, producing a pathologic extracellular matrix of bone and cartilage.[2,10] HO can be further divided by cause into genetic and acquired etiologies[3]. Injury is the main culprits of acquired HO, including musculoskeletal polytrauma, central nervous system trauma, and orthopedic procedures[4-7].

HO around the hip is exceedingly common and may have a dramatic clinical impact[8–10]. This event occurs up to 40%[11-13] after hip arthroplasties, and up to 7% can severely impact the functional outcomes.[1,14] Predisposing factors of HO around the hip are smoking, male gender, hypertrophic osteoarthritis, ankylosing spondylitis, and diffuse idiopathic skeletal hyperostosis.[15] In addition, hip surgical access differentially affects the incidence rate of HO. In general, the use of a postero-lateral and mini-invasive approaches carries a

lower risk of HO compared with anterior and antero-lateral approaches.[16-18] The importance of muscular injury in hip exposure has been suggested by the reduced incidence of HO when the gluteus minimus is resected in the Kocher–Langenbeck surgical approach.[19] Therapeutic approaches to prevent HO and HO after arthroplasty are lacking, and are essentially limited to low-dose radiation treatment or nonsteroidal anti-inflammatory drugs (NSAIDs).[2]

Although many mouse models of HO have been devised, there are no available mouse models of arthroplasty associated with HO. This lack of a tractable model for the study is particularly notable, as arthroplasty is the most common cause of human heterotopic bone formation. Other mouse models of HO include genetic models that mimic fibrodysplasia ossificans progressive (FOP),[20,21] traumatic models after tenotomy,[22] BMP-induced models[23,24] and neurogenic and spinal cord injury models.[25] Here, we present a novel pre-clinical mouse model of post-surgical HO of the hip that reproduces periosteal, intermuscular/intramuscular, and intracapsular locations typical of the human disease. Further, we demonstrate using transgenic reporter animals that post-surgical hip HO is derived from common HO progenitor cells, illustrating the usefulness of this mouse model for future investigation into the cellular and molecular contributors to arthroplasty associated HO.

## Materials and Methods

### Animals and Conditions

All animal procedures were carried out in accordance with the guidelines provided in the Guide for the Use and Care of Laboratory Animals from the Institute for Laboratory Animal Research (ILAR, 2011) and were approved by the Animal Care and Use Committee (ACUC) of the Johns Hopkins University (MO16M334). Throughout the study, mice were housed in an IVC system rack using polypropylene cages (19 cm × 28 cm × 13 cm), with 12/12 night/day cycles, 21 °C (±2°C) and 50% (±20%) relative humidity. All mice had *ad libitum* access to complete mouse food and filtered water.

Wild-type mice C57BL/6J mice were purchased from Jackson Laboratories (Bar Harbor, ME). Pdgfra-CreER$^{T2}$ mice were a kind gift from the Bergles Laboratory at Johns Hopkins, commercially available from The Jackson Laboratory (catalog number 018280). mT/mG mice were purchased from The Jackson Laboratory (catalog number 007576). Pdgfra-CreER$^{T2}$ and mT/mG mice were crossed to generate Pdgfra-CreERT2; mT/mG reporter mice, which were used for all experiments as previously described.[26,27] Tamoxifen (TM; product number T5648; Sigma-Aldrich, St. Louis, MO, USA) was provided by i.p. injection as per previously validated protocols for 5 days consecutively (150 mg/g by weight).[26,28,29] With this previously validated TM-injection schedule, >93.7% fidelity between reporter activity and immunolocalization was previously observed.[28] TM was dissolved in sunflower seed oil. Tail genomic DNA was used for genotyping. Essentially no recombination within the joint-associated tissues was observed with the injection of a TM-free control vehicle. Scleraxis (Scx)-GFP reporter animals were kindly donated by the Farber lab, Oregon Health & Science University. In this model, the open reading frames of the GFP are inserted into the first exon of the Scx gene.[30] Mixed gender, 10–12 week old animals were used for all experiments. In total, $N$ = 8 C57BL/6J, $N$ = 3 Pdgfra-CreERT2; mT/mG reporter mice, and $N$ = 3 Scx-GFP mice were used for the experiments.

### Surgical Procedure

An anterolateral approach to the hip was performed (Fig. 1). Animals were anesthetized with inhaled isoflurane (3–5% induction, 2–3% maintenance) delivered with combined oxygen and nitrous oxide (1:2 ratio) along with the subdermal injection of sustained-release buprenorphine (1.2 mg/kg SC). The animal was placed in a lateral decubitus position on a heated pad and covered to minimize heat loss. The right leg was prepared for surgery: hair was clipped and skin was disinfected with povidone-iodine 5% and alcohol 70%. A 2 cm incision was made centered on the greater trochanter and directed proximal to the iliac crest and distally over the lateral shaft of the femur. The joint was then reached following the intermuscular plane between the rectus femoris and gluteus medius muscles. After capsulotomy was performed, the femoral head was partially dislocated to give access to the acetabular reamer (Cell-point Scientific, MD). Then, the articular cartilage was removed using a reamer of 1.2 mm in diameter (Cell-point Scientific, MD) operated by a micropower drill (Roboz Surgical Instrument Co., MD). The surgical site was then irrigated with saline solution. The gluteus medius and superficial fascia were then re-approximated with Vicryl 5-0 suture (Ethicon Inc, Somerville, NJ) and the skin was then closed with Ethilon 5-0 suture (Ethicon Inc.).

### High-Resolution XR and Microcomputed Tomography (μCT) Assessments

The hip joint was assessed using a combination of high-resolution XR and μCT imaging. First, live high-resolution XR imaging was performed every 2 weeks to assess the skeletal tissues (Faxitron Bioptics, Tucson, AZ). The imaging was then scored using the Brooker classification adapted for the mouse using posteroanterior XR of the hip joint[4] (a scale of 1:40 was adapted which considers the mean length of the femur from mice in comparison to the human adult). Second, general morphological appearance and morphometric analysis were performed using *ex vivo* microCT using a Skyscan 1275 scanner (Bruker-MicroCT, Kontich, Belgium) with the following settings: 65 kV, 153 μA, 1 mm aluminum filter in 180°, 6 frames per 0.3° with a 10 μm voxel size. Images were reconstructed using NRecon and exported as DICOM files. DataViewer software was used to re-align the images and quantitative parameters were assessed using Skyscan CTan software (SkyScan, Kontich, Belgium) as previously published.[31] We used a cylindrical region of interest (ROI) of 4.5 mm in diameter and 3 mm of thickness centered on the femoral head on the axial projection. This ROI has been developed to encompass the main anatomical structures involved in this surgical model procedure: the femoral head, the acetabular bone, and the greater trochanter. A threshold value range of 80-255 was used. After global thresholding was carried out, a 3-dimensional (3D) data analysis including bone volume (BV), bone volume density (BV/TV), bone surface (BS), bone surface in relation to bone volume (BS/BV), bone surface density (BS/TV), and the trabecular number (Tb.N) was performed. The 3D reconstruction was performed using Dragonfly (ORS Inc., Montreal, Canada).

### Histology and Immunohistochemistry

Specimens were harvested and placed in 4% paraformaldehyde (PFA) at 4 °C for 24 h. After sequential washes in PBS, samples were decalcified in 14% EDTA (1:20 volume, Sigma Aldrich) for 60 d at 4 °C. Samples were cryoprotected using 30% sucrose

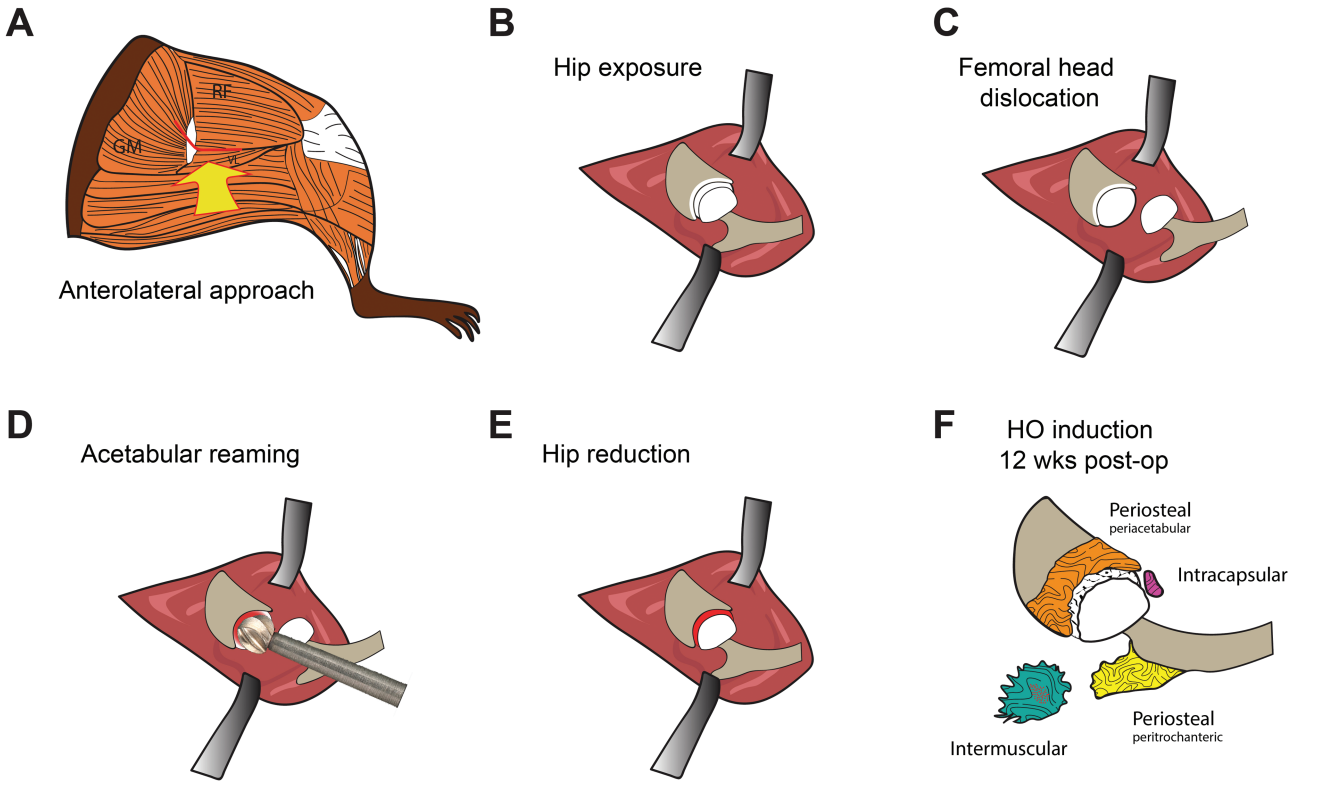


**Figure 1.** Schematic of acetabular reaming to induce heterotopic ossification in the mouse. (**A**–**E**). (**A**) The hip is accessed using an anterolateral approach through the intermuscular plane between the rectus femoris and vastus lateralis, and proximally the gluteus medius. (**B**–**D**) After capsulectomy is carried out, the femoral head is dislocated and the acetabulum is reamed until the articular cartilage is removed. (**E**) The femoral head is reduced into the acetabular cavity and the soft tissue are carefully closed. (**F**) Both periosteal and inter/intramuscular heterotopic bone are observed post-operatively over a 12-week period.

overnight at 4 °C before embedding in OCT (Tissue-Tek 4583, Torrance, CA). Axial sections of the hip joint, starting proximally from the iliac bone and ending distally in the ischium bone were obtained using cryosections at 20 µm thickness. Axial sections were mounted on adhesive slides (Fisherbrand Superfrost Plus, Thermo Fisher Scientific, Waltham, MA). Histochemical stains were performed including routine H&E and Goldner's Modified Trichrome. For detection of fluorescent reporter animals, sections were washed in PBS × 3 for 10 minutes and then mounted with DAPI mounting solution (Vectashield H-1500, Vector Laboratories, Burlingame, CA). For immunohistochemical staining, sections were blocked with 5% goat serum in PBS for 1 h at RT and incubated with primary antibodies (osteocalcin (OCN, 1:200, ab93876), SRY-Box transcription factor 9 (SOX9, 1:200, ab185230), platelet and endothelial cell adhesion molecule 1 (CD31, 1:150, ab28364), Abcam, Cambridge, UK) overnight at 4 °C. Next, Alexa Fluor 647 conjugated secondary antibody (1:200, ab150079, Abcam) was used. Finally, sections were counterstained with DAPI mounting medium.[32] Digital images of these sections were captured with 10–100× objectives using upright fluorescent microscopy (Leica DM6, Leica Microsystems Inc., Buffalo Grove, IL) or confocal microscopy (Zeiss LSM780 FCS, Carl Zeiss Microscopy GmbH, Jena, Germany).

## Fluorescence-Activated Cell Sorting

The periarticular soft tissues were microdissected using either uninjured Pdgfra-CreERT2; mT/mG reporter mice, or reporter animals 7 d after injury. The microdissected tissues were digested using 1 mg/mL collagenase type I (Worthington Biochemical Corporation, Lakewood, NJ; LS004197), 1 mg/mL collagenase type II (Worthington Biochemical Corporation; LS004177), and dispase (2 mg/mL, Sigma–Aldrich, D4693). Cell fractions from sequential digestions 1–6 were collected and resuspended in red blood cell lysis buffer (37 °C for 5 minutes). After centrifugation, cells were resuspended in Hanks' Balanced Salt Solution (HBSS) and 0.5% bovine serum albumin. Flow cytometry was performed to isolate the mGFP$^+$ cell fraction.

## RT2 Profiler PCR Array

According to the manufacturer's protocol, real-time PCR was performed using RT$^2$ Profiler PCR Arrays in combination with RT$^2$ SYBR Green ROX qPCR Mastermix (Qiagen). A total of 70 ng RNA of freshly isolated Pdgfra-mGFP$^+$ cells were used for first-strand cDNA synthesis. A total of 5 µL first-strand cDNA synthesis reaction was used to prepare the pre-amplification mix. When cycling was finished, 2 µL of Side Reaction Reducer was added to each pre-amplified reaction. The products were incubated at 37 °C for 15 minutes, followed by heat inactivation at 95 °C for 5 minutes and the addition of 84 µL of nuclease-free water. A 102-µL cDNA synthesis reaction volume was mixed with 2× RT2 SYBR Green Mastermix and RNase-free water to obtain a total volume of 1100 µL. Subsequently, 10µL of the PCR component mix was placed into each well of the PCR array. The 3 steps of the cycling program were 95 °C for 10 minutes for 1 cycle, followed by 40 cycles of 95 °C for 15 s and 60 °C for 60 s. This process was repeated for 40 cycles using the ABI-QuantStudio 5 (Applied Biosystems, Waltham, MA, USA). The expression levels were quantified relative to the values obtained for

housekeeping genes. Data analyses were performed using web-based analysis software (https://dataanalysis2.qiagen.com/pcrhttps://dataanalysis2.qiagen.com/pcr).

### Statistical Analysis

Results are expressed as the mean ± 1 SD. Following an *F*-test of the homogeneity of the variances, a Student's *t*-test was used for two-sample comparisons. A one-way ANOVA with Tukey's multiple comparisons test was used for more than 2 group comparisons (Graphpad Software 8.1). Pearson's correlation coefficient *r* was used to assess the association between 2 continuous variables. Sample size for in vivo experiments was calculated using the G*Power software (latest ver. 3.1.9.7; Heinrich-Heine-Universität Düsseldorf, Düsseldorf, Germany; http://www.gpower.hhu.de/). A 2-sample *t*-test with $n = 8$ biologic replicates per group provided an 80% power to detect effect sizes of at least 1.6 assuming a 2-sided 0.05 level of significance. $^{*}P < .05$ and $^{**}P < .01$ were considered significant.

## Results

### Acetabular Reaming Induces Periarticular Heterotopic Ossification Phenocopying Human Disease

After acetabular reaming, mice were surveilled by high-resolution roentgenography (Fig. 2). Periosteal reactive bone formation as well as radiodensity within the periarticular soft tissues was uniformly apparent in all mice as early as 4 weeks post-operatively (Fig. 2A). Progressive ossification as well as joint space narrowing was observed over the 12-week period. The final XR images were then staged according to a Brooker classification system adapted for mice[4] (Fig. 2B). The majority of animals demonstrated stage 2 heterotopic bone, as defined by new bone formations arising from the iliac and femoral locations leaving at least 300 µm between the opposing surfaces (62.5%, 5/8 mice). A total of 25% of cases demonstrated stage 3 HO, characterized by new bone formations arising from the iliac and femoral locations leaving less than 300 µm between the opposing surfaces (2/8 mice). A total of 12.5% of cases showed stage 1 HO, characterized by small areas of calcified tissues (1/8 mice) (Table 1).

### Micro Computed Tomography (µCT) Analysis Demonstrates Heterogeneity in Periarticular HO Sites

After hip arthroplasty in humans, a variety of soft tissues may show ossification, including the muscles, entheses, capsule remnants, and periosteum. To assess the specific locations of HO formation after acetabular reaming in the mouse, we next used high-resolution µCT imaging at the study endpoint (Fig. 3). 3-dimensional µCT reconstructions of a representative

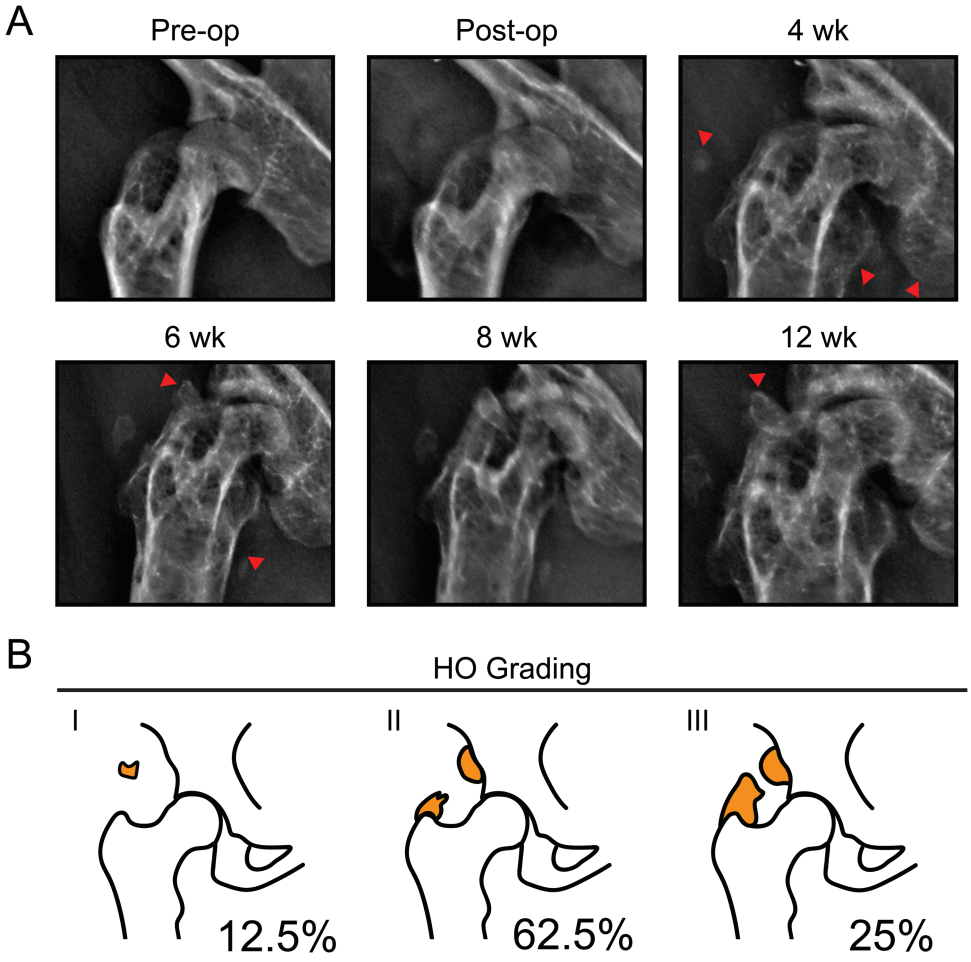


**Figure 2.** Acetabular reaming induces heterotopic bone as seen in human patients. Animals were treated with acetabular reaming to induce heterotopic ossification (HO) and then followed with in vivo high-resolution roentgenography (XR) at up to 12 weeks post-operatively. (**A**) Representative XR of the treated hip, pre-operatively, immediately postoperatively, and at 4, 6, 8, and 12 weeks post-operative. (**B**) Heterotopic ossification (HO) staging according to the Brooker classification. The relative incidence is reported for each stage. *N* = 8 animals in total.

pelvic bone showed abundant periarticular heterotopic bone in several regions of the treated hip (Fig. 2A). Intracapsular HO was observed in 4/8 cases—with anterior or posterior locations in relation to the femoral neck, and in proximity to the acetabular labarum (Fig. 3B, 3E). Abundant periosteal HO was observed across all samples (8/8 cases) (Fig. 3F, 3I). The majority of cases demonstrated periosteal reactive bone on the femur located mainly at the greater trochanter especially surrounding muscle insertions. Inter/intramuscular HO was observed in 6/8 cases (Fig. 3J, 3M). Muscle-associated HO was observed most often involving the gluteus medius (6/8 cases), while extension and involvement of the extra rotator muscles and rectus femoris were also seen (2/8 and 2/8 cases, respectively). Subchondral bone sclerosis with a reduction of

**Table 1.** Grading of HO according to Brooker classification

| Grade | Number | % |
|---|---|---|
| 4 | 0 | 0 |
| 3 | 2 | 25 |
| 2 | 5 | 62.5 |
| 1 | 1 | 12.5 |

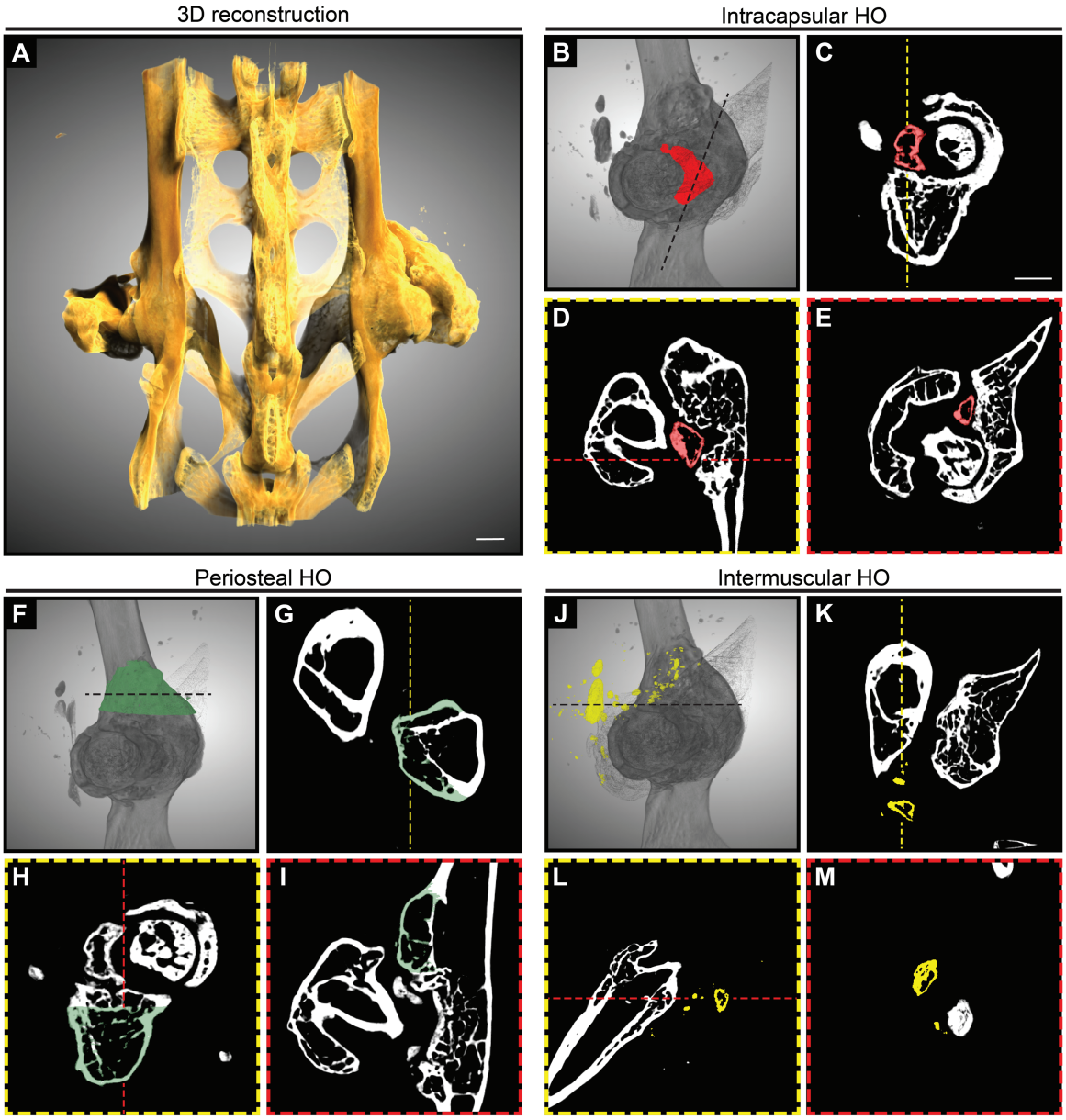


**Figure 3.** Micro-computed tomography (μCT) illustration of heterotopic ossification after acetabular reaming. Animals were treated with acetabular reaming to induce heterotopic ossification (HO) and analyzed with ex vivo μCT at 12 weeks post-operatively. (**A**) Representative 3-dimensional (3D) μCT reconstructions of the pelvis of a treated animal at 12 weeks post-operative, shown from a posterior perspective. (**B**–**E**) Representative μCT reconstructions showing intracapsular HO, are shown in red. (**B**) 3D reconstruction of the acetabular bone, with the femur shown in shadow. (**C**) Coronal, (**D**) sagittal, and (**E**) axial cross-sections. (FI) Representative μCT reconstructions showing periosteal HO, appearing green. (**F**) 3D reconstruction of the acetabulum. (**G**) Axial, (**D**) sagittal, and (**E**) coronal sections. (**J**–**M**) Representative μCT reconstructions showing intermuscular HO, appearing yellow. (**J**) 3D reconstruction of the acetabulum. (**K**) Axial, (**L**) sagittal, and (**M**) coronal cross-sections. White scale bar: 1 mm.

the joint space was a universal feature and was suggestive of osteoarthritis (OA) changes.

The extent and variability in the burden of disease were further assessed by quantitative μCT analysis across all animals. Assessments included analysis of bone volume (BV), bone volume density (BV/TV), and bone surface (BS), bone surface in relation to bone volume (BS/BV), bone surface density (BS/TV), and the trabecular number (Tb.N) (Fig. 4). Here, the treated hip resulted in a significant increase in nearly all quantitative metrics in relation to the contralateral limb (61–63% increase across measured parameters). A non-significant trend toward an increase in BS/BV was observed. We next examined the extent to which the quantitative burden of disease by microCT correlated with the previously calculated Brooker stage (Table 2). While some variability in the distribution across samples was observed, a strong and significant correlation between Brooker stage and μCT measurements was noted (Table 2).

## Acetabular Reaming Induced Mature Bone Matrix in Several Locations

Histological analyses were next performed, which further confirmed the presence and extent of periarticular heterotopic bone (Fig. 5). A combination of H&E staining and Goldner's Modified Trichrome (GMT) staining was performed. Histologic assessments of periosteal-based HO observed thick trabeculae of bone that extended off the native iliac and femoral cortices (Fig. 5A, 5D). A combination of woven and lamellar bone was observed at the 12-week time point. A new bone marrow space was also consistently observed between the neo-cortex and native cortex across samples. Intramuscular HO was next assessed (Fig. 5E, 5H). Overall, heterotopic bone was less exuberant, but still readily appreciated by histology. Nodules of bone were most common in intermuscular fascial planes but were also found within the muscle belly of the gluteus medius in some cases. Larger nodules of heterotopic bone demonstrated an eggshell-type pattern of thin peripheral ossification with the central bone marrow cavity (Fig. 5G), while smaller nodules of solid bone were also seen (Fig. 5H). Thus, histologic analysis confirmed the presence and stereotypical appearance of heterotopic bone after acetabular reaming.

## PDGFRα-expressing Cellular Descendants Give Rise to Heterotopic Bone After Acetabular Reaming

Stromal cells typified by expression of the platelet-derived growth factor (PDGF) receptor PDGFRα have been found to give rise to HO at intramuscular and intratendinous

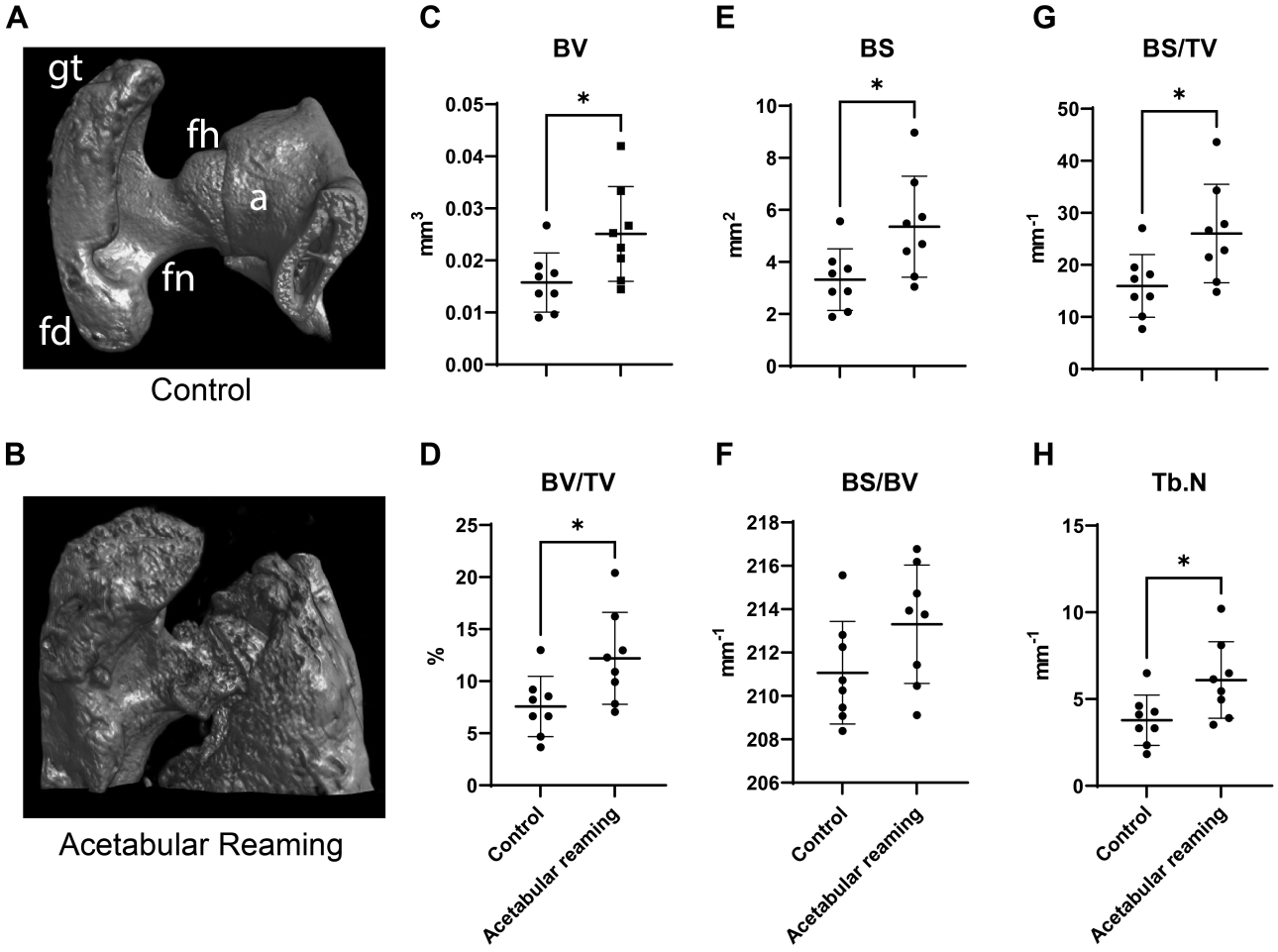


**Figure 4.** Quantitative μCT analysis of the new bone formation. Animals were treated with acetabular reaming to induce heterotopic ossification (HO), and analyzed with ex vivo μCT at 12 weeks post-operatively. A cylindrical region of interest (ROI) was used (4.5 mm diameter, 3 mm thickness, centered on the femoral head within an axial projection. fh: femoral head; fn: femoral neck; gm: fd: femoral diaphysis; gt: greater trochanter. (**A**, **B**) Representative images of the structures considered in the bone analysis of control and treated groups, including the femoral head, acetabular bone, and the greater trochanter. (**C**–**G**) Quantitative μCT analysis of the hip joint, including (**C**) bone volume (BV), (**D**) fractional bone volume (BV/TV), (**E**) bone surface (BS), (**F**) bone surface in relation to bone volume (BS/BV), (**G**) bone surface density (BS/TV), and (**H**) the trabecular number (Tb.N). Dots in scatterplots represent an individual joint, while crosshairs and whiskers represent mean and one SD, respectively. *$P < .05$.

**Table 2.** Correlation of μCT results and Brooker grading

| μCT parameter | *R* | $R^2$ | 95% CI | *P* value |
|---|---|---|---|---|
| BV | 0.9209 | 0.8481 | 0.6160–0.9858 | <.01 |
| BV/TV | 0.9207 | 0.8477 | 0.6151–0.9858 | <.01 |
| BMD | 0.9186 | 0.8438 | 0.6064–0.9854 | <.01 |

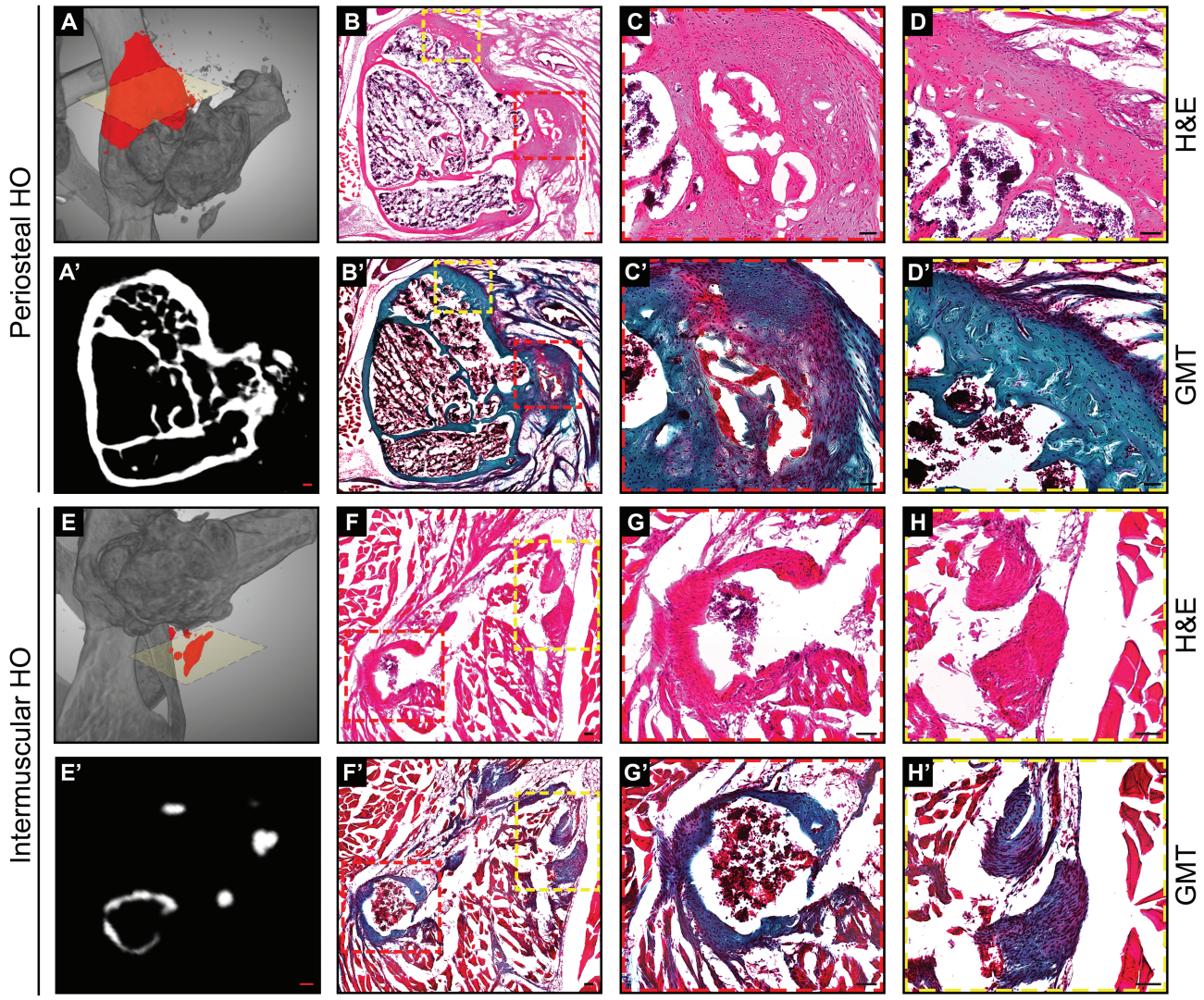


**Figure 5.** Histologic illustration of heterotopic ossification following acetabular reaming. Histological analysis at 12 weeks after acetabular reaming, to examine periosteal and intermuscular heterotopic ossification (HO). (**A**–**D**′) Representative images showing the new periosteal bone formation in the iliac bone. (A) Three-dimensional (3D) μCT reconstructions showing in red the area of interest. (A′) Axial μCT cross-section. (B-D) H&E staining and (B′-D′) Goldner's Modified Trichrome (GMT) staining. The bone matrix appears blue/green, while osteoid and muscles appear red. (E-H′) Representative images showing the ectopic bone formation among the muscular structures. (E) 3D μCT reconstructions showing in red the area of interest. (E′) Axial μCT cross-section. (F-H) H&E staining and (F′-H′) GMT staining. Black scale bars: 50 μm; Red scale bars: 100 μm.

sites.[3,26,33] We sought to determine if periarticular HO after acetabular reaming likewise demonstrates a cellular contribution from the descendants of PDGFRα-expressing cells (Fig. 6). Here, inducible PDGFRα reporter animals were examined (PDGFRα$^{mT/mG}$ reporter mice), in which tamoxifen administration and washout were provided 2 weeks before surgery (Fig. 6A). 3 weeks after surgery, reporter activity was assessed within uninjured and injured hips (PDGFRα expressing cells and their cellular descendants appear green, while all other cells appear red). Within the uninjured hip (Fig. 6B), skeletal sites of reporter activity were found in the femoral and acetabular articular cartilage, periosteum, tendons, and their entheses. These findings were in agreement with prior observations in the murine stifle joint.[27] Extraskeletal sites of PDGFRα reporter activity were likewise consistent with prior reports,[26,27] including the perineurium, perivascular spaces, and intermuscular connective tissue.

In the injured hip, a conspicuous increase in PDGFRα reporter activity was observed 3 weeks after injury in areas with reactive changes and HO (Fig. 6C). The removal of the

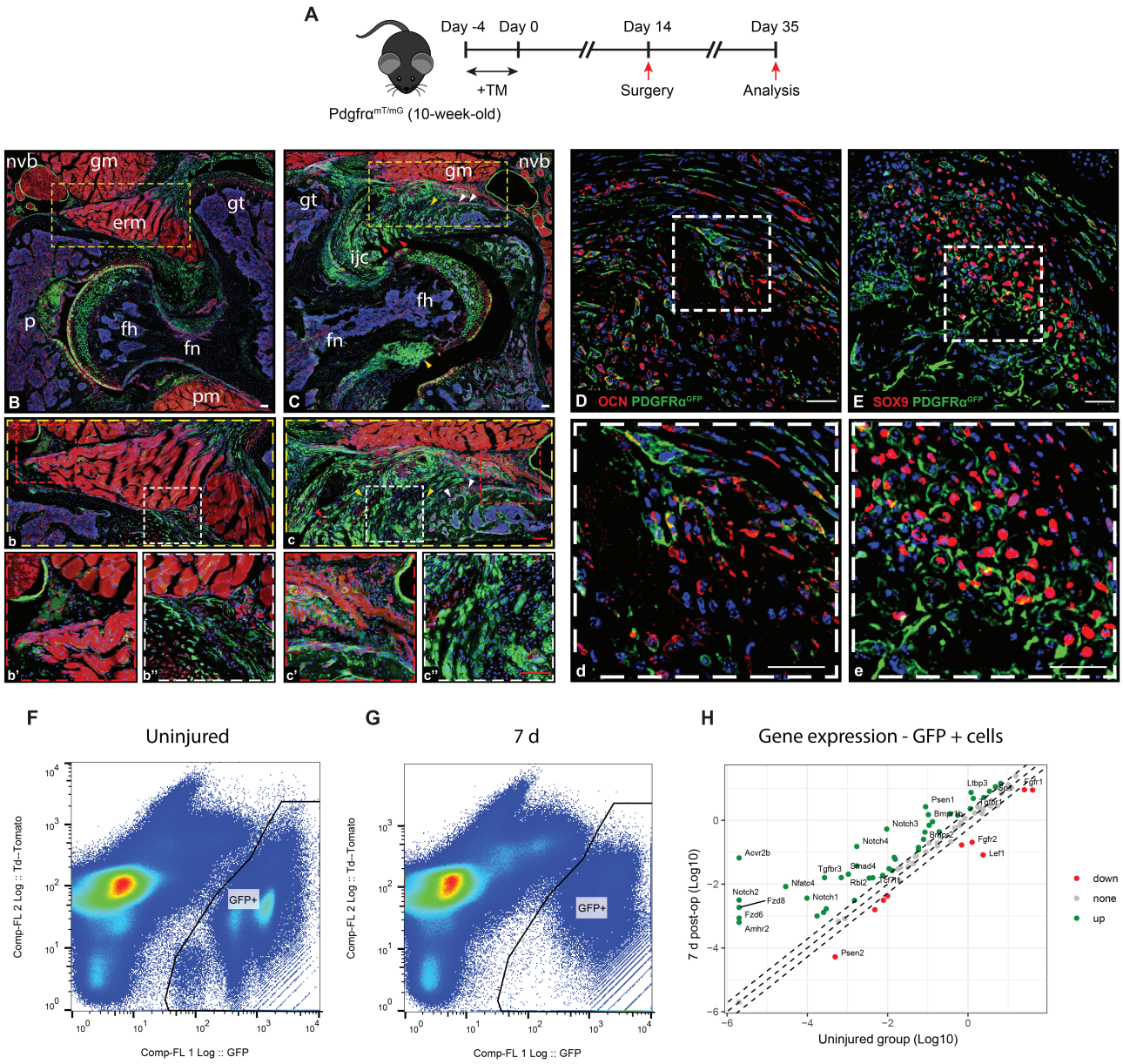


**Figure 6.** PDGFRα expressing cells give rise to the heterotopic bone after acetabular reaming. (**A**) PDGFRαmT/mG reporter animals underwent induction of heterotopic ossification (HO) by acetabular reaming, followed by analysis at 3 weeks post-operatively. Tamoxifen labeling was performed 14 d prior to surgery. PDGFRα+ cells and their progeny appear green, while all other cells appear red. (**B**) Axial section is taken from an uninjured hip. erm: extrarotators muscles; fh: femoral head; fn: femoral neck; gm: gluteus medius muscle; gt: greater trochanter; nvb: neurovascular bundle; p: pulvinar. (b-b'') high magnification pictures showing more in detail the normal structure near the neurovascular bundle (b') and the tissue interposed between the acetabular bone and the extrarotator muscle complex. (**C**) Axial section obtained 3 weeks after HO induction, demonstrating the newly formed heterotopic bone (white arrowheads) in the periacetabular area in proximity to the neurovascular structures (C-c'), including chondroid (yellow arrowheads) (C, c'') and fibroproliferative (red arrowheads) areas. Co-staining with OCN (D-d) and SOX 9 (**E**-e) confirmed the osteochondral commitment of PDGFR-alpha expressing cells. DAPI nuclear counterstain appears blue. (**F**) Flow cytometry plots of microdissected peri-acetabular tissues among uninjured and (**G**) 7 d post-injury PDGFRαmT/mG reporter animals. Td tomato positive cells are shown on the left and GFP expressing cells are shown on the right of the plots. (**H**) Gene expression in Log 10 among injured and control PDGFRα-mGFP+ cells. Each dot represents one gene with green ones representing 2-fold higher expressed in 7 d group and red ones represent 2-fold lower expressed genes after injury. The gray dots represent genes within 2-fold cutoff threshold. The dashed lines represent −2, 0, and +2 fold change, respectively. *N* = 8 animals used, 3 for 7 d and 5 for the uninjured group. Red scale bars: 100 μm, white scale bars: 20 μm.

articular surface on the acetabular side was confirmed by the absence of reporter activity in this area (Fig. 6C). An increased mGFP reporter activity was noted in the periarticular tissues (Fig. 6c) with new cartilage and new bone formation associated with the iliac bone (1.4-fold increase, Fig. 6c''). Notably, an expansion of PDGFRα reporter$^+$ cells was also noted in the tissue surrounding the large nervous trunks (1.2-fold increase, Fig. 6c'). The commitment to an osteochondrogenic lineage of PDGFRα-expressing cells in periarticular tissues was confirmed by Osteocalcin (OCN) (Fig. 6D, d) and SOX9 immunostaining (Fig. 6E, e). OCN immunohistochemical staining showed clear areas of overlap with PDGFRα reporter activity, although relatively frequent OCN$^+$ reporter$^-$ cells were also found (Fig. 6D, d). Likewise, nuclear SOX9

immunostaining was present in many cells which appeared to have membranous PDGFRα reporter activity (Fig. 6E, e). Safranin O staining confirmed the presence of cartilage in these areas, both intracapsular and extracapsular locations (Supplementary Fig. S1). In addition, the spatial relationship between PDGFRα-expressing cells and vascular structures using CD31immunostaining was confirmed (Supplementary Fig. S2 A, A'). Thus, cellular descendants of PDGFRα$^+$ cells gave rise, at least in part, to HO after acetabular reaming, in similarity to previously devised experimental HO models at other anatomical sites.

Having noted that a significant number of PDGFRα-mGFP$^+$ cells express osteochondral antigens at the HO site, we next examined the acute change in the transcriptome of these cells after injury. For this purpose, FACS isolation of periarticular PDGFRα-mGFP$^+$ cells was performed 7 d after HO induction. Analysis of genes related to mesenchymal progenitor cell stemness and differentiation was performed using a PCR array, in comparison to uninjured control PDGFRα-mGFP$^+$ cells (Fig. 6F, 6G). Among 84 total genes, 50% showed a 2-fold increase and 11% showed a 2-fold decrease in expression after HO induction. Prominent changes were notable in BMP, TGFβ, and Notch signaling components, which were clearly upregulated at 7 d post-injury. Some of the most expressed genes were *Acvr2b* (32,145.05-fold-change), *Notch2* (1526.94 FC), *Fdz8* (897.30 FC), *Fdz6* (415.89 FC), *Amhr2* (305.84 FC), *Tgfbr3* (59.67 FC), *Smad4* (19.57 FC) and *Bmpr1b* (14.63 FC) (Fig. 6H, see Supplementary Table S2 for a complete gene list). Thus, HO induction via acetabular reaming leads to a change in the transcriptional profile of PDGFRα-mGFP$^+$ cells, including several signaling pathways associated with osteochondrogenic differentiation.

## Scleraxis Expressing Cells Mark the Areas That Give Rise to HO

Scleraxis (Scx) expressing cells have also been reported to give to HO, especially at sites of ligaments and tendons.[6,8] The distribution of Scx expressing cells was examined in injured and uninjured joints, using Scx-GFP reporter animals. 3 weeks after acetabular reaming, the distribution of GFP$^+$ stromal cells were studied (Fig. 7A-b'). In the normal hip (Fig. 7A), tendons and some periosteum (Fig. 7a') were the main locations of Scx-GFP$^+$ cells. In the injured hip (Fig. 7B), a conspicuous increase

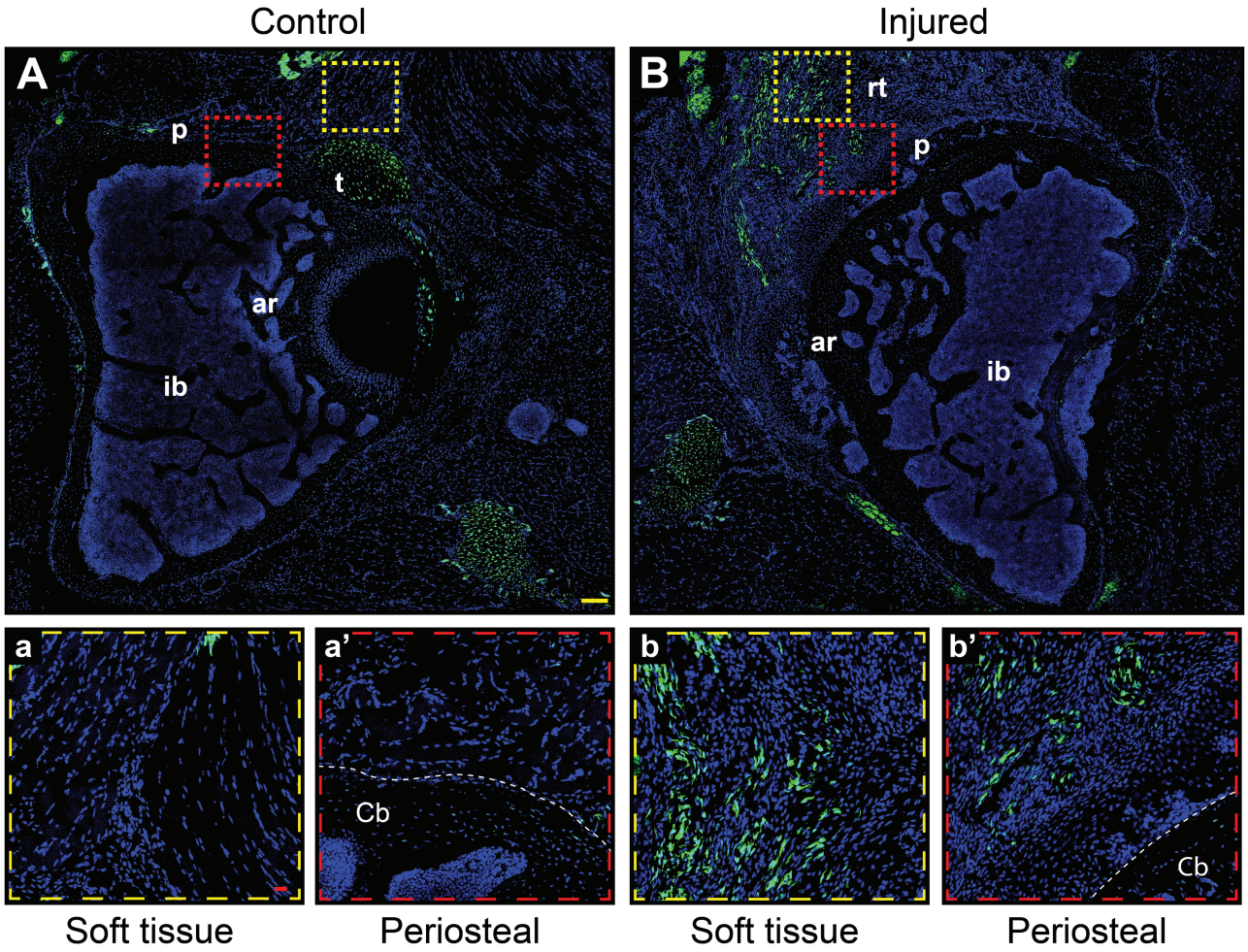


**Figure 7.** Scleraxis expressing cells mark the areas that give rise to the heterotopic bone. Scleraxis (Scx)-GFP reporter animals underwent induction of heterotopic ossification (HO) by acetabular reaming, followed by analysis at 3 weeks post-operatively. Scx-GFP+ cells appear green. (**A**) Axial section taken from an uninjured hip (A-a') with high magnification pictures showing more in detail the soft tissue (a) and periosteal (a') areas. (**B**-b') Axial section obtained 3 weeks after HO induction, demonstrating heterotopic bone in the soft tissue and periosteal periacetabular areas (b-b'). Abbreviations: p, periosteum area; t, tendon; ar, acetabular roof; ib, iliac bone; rt, reactive tissue; cb, cortical bone. DAPI nuclear counterstain appears blue. Yellow scale bar: 100 μm. Red scale bars: 20 μm.

in GFP+ reporter activity was noted in the soft tissues and periosteal areas, coinciding with areas of new cartilage formation (Fig. 7b, b'). Sox9 immunostaining confirmed overlap with Scx expressing cells (Supplementary Fig. S3). Thus, and in keeping with our prior observations in ligamentous and tendinous HO models, Scx reporter expressing cells were present within the HO site after acetabular reaming.

## Discussion

Heterotopic ossification (HO) is a diverse set of pathologies, of which joint-associated HO after elective surgery is particularly common.[34] In some instances, arthroplasty-associated HO has a frequency of up to 40% of cases.[2] We present a mouse model of hip dislocation and acetabular reaming that mimics elements of human arthroplasty and induces periarticular HO with 100% penetrance. The diverse locations of HO in this mouse model (intracapsular, inter/intramuscular, and periosteal) phenocopy human periarticular HO after arthroplasty.

Although models of trauma-induced HO have been devised, including tendon injury,[35,36] blast injury,[37,38] and traumatic amputation,[39,40] this is the first mouse model of post-surgical hip HO. Previous models, such as the well-established burn tenotomy have significantly contributed to the biology of HO, but are not necessarily encountered clinically.[36] In this perspective, acetabular reaming could represent a potentially important model for future testing of therapies, as arthroplasty-associated HO is by far one of the most common etiologies in human patients.

HO cell progenitors have multiple derivations. Bone marrow, periosteum, entheses, fascia, and reaming fragments can differentially contribute to the genesis of HO. We were interested to observe that commonly designated HO progenitor cells, including PDGFRα -expressing cells and Scx-expressing cells, give rise to peri-joint HO in our model. PDGFRα -expressing cells, have been shown to similarly give rise to intramuscular HO,[41] and tendinous HO.[42] Basal expression of PDGFRα reporter activity is present within multiple cells capable of bone formation, including perivascular adventitial cells,[26] perineural cells,[26] intra-articular, and periarticular ligaments,[27] and in some periosteal cells.[43] Interesting, in our prior work we observed that the frequency of PDGFRα+ cells especially within the perivascular space differs somewhat widely across organs.[26] Some vascularized tissue sites are enriched for PDGFRα+ adventitial perivascular cells (eg, aorta, skeletal muscle, and adipose tissue), while several visceral sites showed infrequent PDGFRα+ adventitial cells (eg, liver and lung). Interestingly, these high-frequency PDGFRα+ tissue depots are also well-described sites of heterotopic ossification.[2,44] Conversely, other tissues with a rare frequency of PDGFRα+ adventitial cells represent tissues that rarely develop ectopic bone (eg, viscera such as the liver).[2] This interesting parallel could be one explanation for the tendency of certain tissue types to accumulate ectopic bone under pathologic contexts. Admittedly, diverse reporter systems have been used to mark HO progenitor cells, including for example Prx1,[8] Mx1,[6] Gli1,[45] and Wnt1[46] among others. Dissection of the relative cellular contributions to HO within this newly developed periarticular model will be an ongoing task.

The current study has several limitations. First, we performed relatively early (1 and 3 weeks) and later timepoints (12 weeks), but intermediate timepoints were not performed. In the future, a more complete spectrum of the HO phenotype induced by acetabular reaming would benefit from intermediate timepoints as well. Second, the cellular origins of periarticular HO are only beginning to be understood. For example, PDGFRα reporter activity was present in numerous distinct mesenchymal cell types in this model, and reporter models with more limited distributions are needed to further clarify the cellular origins of periarticular HO. Alternatively, advanced technologies like single-cell RNA-seq would be beneficial to more clearly -decipher the cellular origins and heterogeneity of composition of periarticular HO. Third, we used the contralateral limb as a control throughout the present work. In future work, the utilization of sham-operated limbs could be incorporated as an additional control. Finally, the rate of occurrence of HO in this model (100%) well exceeds that of arthroplasty in human patients. Although this reliability in HO formation is an experimental advantage, its limitations as a faithful model for human disease must be acknowledged.

In summary, the proposed model induces periarticular HO in the mouse with defined cellular contributors similar to other experimental HO models. This protocol may be used in the future for further detailing of the cellular and molecular mediators of post-surgical HO, as well as the screening of new therapies.

## Acknowledgment

A.W.J. was supported by the NIH/NIAMS (R01 AR070773), NIH/NIDCR (R21 DE027922), Department of Defense (W81XWH-18-1-0336, W81XWH-18-10613, W81XWH-20-1-0795, W81XWH-20-1-0302), American Cancer Society (Research Scholar Grant, RSG-18-027-01-CSM), and the Maryland Stem Cell Research Foundation (2019-MSCRFD-5074). The content of this article is solely the responsibility of the authors and does not necessarily represent the official views of the National Institutes of Health, Department of Defense, or U.S. Army. A.W.J. is a paid consultant for Novadip and Lifesprout. This arrangement has been reviewed and approved by Johns Hopkins University in accordance with its conflict of interest policies. A.W.J. receives funding for unrelated research from Novadip. B.L. was supported or partially supported by National Institutes of Health (NIH) R01GM123069, R01AR071379, and R61 AR078072-01, American College of Surgeons Clowes Award, and U.S. Department of Defense Grant W81XWH-18-1-0653 (OR170174) and W81XWH-19-PROP-ARA (OR190048).

## Conflict of Interest

A.S.L. declared ownership interest in Ensysce Biosciences, unrelated to the scope of the current manuscript. A.W.J. declared an advisory role with Lifesprout and Novadip LLC. All of the other authors declared no potential conflicts of interest.

## Author Contributions

S.N., Y.W.: collection and/or assembly of data, data analysis, and interpretation, manuscript writing; Z.L., Q.Q., S.L., M.C., J.X., G.C.Y.H., R.J.T., B.P., A.L., E.M., B.L.: collection and/or assembly of data, data analysis, and interpretation;

A.W.J.: collection and/or assembly of data, data analysis, and interpretation, manuscript writing, final approval of manuscript, conception, and design, financial support.

## Data Availability

The data that support the findings of this study are available on request from the corresponding author.

## Supplementary Material

Supplementary material is available at *Stem Cells Translational Medicine* online.

## References


1. Riegler HF, Harris CM. Heterotopic bone formation after total hip arthroplasty. *Clin Orthop Relat Res*. 1976;(117):209-216.
2. Meyers C, Lisiecki J, Miller S, et al. Heterotopic ossification: a comprehensive review. *JBMR Plus*. 2019;3(4):e10172. https://doi.org/10.1002/jbm4.10172
3. Agarwal S, Loder S, Brownley C, et al. Inhibition of Hif1alpha prevents both trauma-induced and genetic heterotopic ossification. *Proc Natl Acad Sci USA*. 2016;113(3):E338-E347. https://doi.org/10.1073/pnas.1515397113
4. Agarwal S, Loder SJ, Cholok D, et al. Scleraxis-lineage cells contribute to ectopic bone formation in muscle and tendon. *Stem Cells*. 2017;35(3):705-710.
5. Loder SJ, Agarwal S, Chung MT, et al. Characterizing the circulating cell populations in traumatic heterotopic ossification. *Am J Pathol*. 2018;188(11):2464-2473. https://doi.org/10.1016/j.ajpath.2018.07.014
6. Dey D, Bagarova J, Hatsell SJ, et al. Two tissue-resident progenitor lineages drive distinct phenotypes of heterotopic ossification. *Sci Transl Med*. 2016;8(366):366ra163. https://doi.org/10.1126/scitranslmed.aaf1090
7. Agarwal S, Loder SJ, Brownley C, et al. BMP signaling mediated by constitutively active Activin type 1 receptor (ACVR1) results in ectopic bone formation localized to distal extremity joints. *Dev Biol*. 2015;400(2):202-209. https://doi.org/10.1016/j.ydbio.2015.02.011
8. Agarwal S, Loder SJ, Cholok D, et al. Scleraxis-lineage cells contribute to ectopic bone formation in muscle and tendon. *Stem Cells*. 2017;35(3):705-710. https://doi.org/10.1002/stem.2515
9. Kan L, Peng CY, McGuire TL, et al. Glast-expressing progenitor cells contribute to heterotopic ossification. *Bone*. 2013;53(1):194-203. https://doi.org/10.1016/j.bone.2012.12.008
10. Cocks M, Mohan A, Meyers CA, et al. Vascular patterning in human heterotopic ossification. *Hum Pathol*. 2017;63:165-170. https://doi.org/10.1016/j.humpath.2017.03.005
11. Brooker AF, Bowerman JW, Robinson RA, et al. Ectopic ossification following total hip replacement. Incidence and a method of classification. *J Bone Joint Surg Am*. 1973;55(8):1629-1632.
12. Spinarelli A, Patella V, Petrera M, et al. Heterotopic ossification after total hip arthroplasty: our experience. *Musculoskelet Surg*. 2011;95(1):1-5. https://doi.org/10.1007/s12306-010-0091-6
13. Bedi A, Zbeda RM, Bueno VF, et al. The incidence of heterotopic ossification after hip arthroscopy. *Am J Sports Med*. 2012;40(4):854-863. https://doi.org/10.1177/0363546511434285
14. Regis D, Sandri A, Sambugaro E. Incidence of heterotopic ossification after surface and conventional total hip arthroplasty: a comparative study using anterolateral approach and indomethacin prophylaxis. *Biomed Res Int*. 2013;2013:1-4.
15. Lewis PC, Camou E, Wofford K. The impact of cigarette smoking on the formation of heterotopic ossification among service members with a traumatic amputation. *Mil Med*. 2017;182(5):e1742-e1748. https://doi.org/10.7205/MILMED-D-16-00350
16. Hurlimann M, Schiapparelli FF, Rotigliano N, et al. Influence of surgical approach on heterotopic ossification after total hip arthroplasty—is minimal invasive better? A case control study. *BMC Musculoskelet Disord*. 2017;18(1):27. https://doi.org/10.1186/s12891-017-1391-x
17. Morrey BF, Adams RA, Cabanela ME. Comparison of heterotopic bone after anterolateral, transtrochanteric, and posterior approaches for total hip arthroplasty. *Clin Orthop Relat Res*. 1984;(188):160-167.
18. Tippets DM, Zaryanov AV, Vincent Burke W, et al. Incidence of heterotopic ossification in direct anterior total hip arthroplasty: a retrospective radiographic review. *J Arthroplasty*. 2014;29(9):1835-1838. https://doi.org/10.1016/j.arth.2014.04.027
19. Rath EM, Russell GV Jr., Washington WJ, et al. Gluteus minimus necrotic muscle debridement diminishes heterotopic ossification after acetabular fracture fixation. *Injury*. 2002;33(9):751-756.
20. Hatsell SJ, Idone V, Wolken DM, et al. ACVR1R206H receptor mutation causes fibrodysplasia ossificans progressiva by imparting responsiveness to activin A. *Sci Transl Med*. 2015;7(303):303ra137. https://doi.org/10.1126/scitranslmed.aac4358
21. Lees-Shepard JB, Yamamoto M, Biswas AA, et al. Activin-dependent signaling in fibro/adipogenic progenitors causes fibrodysplasia ossificans progressiva. *Nat Commun*. 2018;9(1):471. https://doi.org/10.1038/s41467-018-02872-2
22. Peterson JR, Okagbare PI, De La Rosa S, et al. Early detection of burn induced heterotopic ossification using transcutaneous Raman spectroscopy. *Bone*. 2013;54(1):28-34. https://doi.org/10.1016/j.bone.2013.01.002
23. James AW, Zara JN, Zhang X, et al. Perivascular stem cells: a prospectively purified mesenchymal stem cell population for bone tissue engineering. *Stem Cells Transl Med*. 2012;1(6):510-519. https://doi.org/10.5966/sctm.2012-0002
24. Liu X, Kang H, Shahnazari M, et al. A novel mouse model of trauma induced heterotopic ossification. *J Orthop Res*. 2014;32(2):183-188.
25. Genet F, Kulina I, Vaquette C, et al. Neurological heterotopic ossification following spinal cord injury is triggered by macrophage-mediated inflammation in muscle. *J Pathol*. 2015;236(2):229-240. https://doi.org/10.1002/path.4519
26. Wang Y, Xu J, Meyers CA, et al. PDGFRalpha marks distinct perivascular populations with different osteogenic potential within adipose tissue. *Stem Cells*. 2020;38(2):276-290. https://doi.org/10.1002/stem.3108
27. Sono T, Hsu CY, Wang Y, et al. Perivascular fibro-adipogenic progenitor tracing during post-traumatic osteoarthritis. *Am J Pathol*. 2020;190(9):1909-1920. https://doi.org/10.1016/j.ajpath.2020.05.017
28. Kang SH, Fukaya M, Yang JK, et al. NG2+ CNS glial progenitors remain committed to the oligodendrocyte lineage in postnatal life and following neurodegeneration. *Neuron*. 2010;68(4):668-681. https://doi.org/10.1016/j.neuron.2010.09.009
29. Sono T, Hsu CY, Negri S, et al. Platelet-derived growth factor receptor-beta (PDGFRbeta) lineage tracing highlights perivascular cell to myofibroblast transdifferentiation during post-traumatic osteoarthritis. *J Orthop Res*. 2020;38(11):2484-2494.
30. Pryce BA, Brent AE, Murchison ND, et al. Generation of transgenic tendon reporters, ScxGFP and ScxAP, using regulatory elements of the scleraxis gene. *Dev Dyn*. 2007;236(6):1677-1682. https://doi.org/10.1002/dvdy.21179
31. Negri S, Wang Y, Sono T, et al. Human perivascular stem cells prevent bone graft resorption in osteoporotic contexts by inhibiting osteoclast formation. *Stem Cells Transl Med*. 2020;9(12):1617-1630. https://doi.org/10.1002/sctm.20-0152
32. Negri S, Wang Y, Sono T, et al. Systemic DKK1 neutralization enhances human adipose-derived stem cell mediated bone repair. *Stem Cells Transl Med*. 2021;10(4):610-622.
33. Wosczyna MN, Biswas AA, Cogswell CA, et al. Multipotent progenitors resident in the skeletal muscle interstitium exhibit robust BMP-dependent osteogenic activity and mediate heterotopic

ossification. *J Bone Miner Res*. 2012;27(5):1004-1017. https://doi.org/10.1002/jbmr.1562
34. Regis D, Sandri A, Sambugaro E. Incidence of heterotopic ossification after surface and conventional total hip arthroplasty: a comparative study using anterolateral approach and indomethacin prophylaxis. *Biomed Res Int*. 2013;2013:1-4.
35. Howell K, Chien C, Bell R, et al. Novel model of tendon regeneration reveals distinct cell mechanisms underlying regenerative and fibrotic tendon healing. *Sci Rep*. 2017;7:45238. https://doi.org/10.1038/srep45238
36. Peterson JR, Agarwal S, Brownley RC, et al. Direct mouse trauma/burn model of heterotopic ossification. *J Vis Exp*. 2015;(102):e52880.
37. Williams DL, Epperson RT, Taylor NB, et al. System setup to deliver air impact forces to a sheep limb: preparation for model development of blast-related heterotopic ossification. *JMIR Res Protoc*. 2019;8(2):e12107. https://doi.org/10.2196/12107
38. Alfieri KA, Forsberg JA, Potter BK. Blast injuries and heterotopic ossification. *Bone Joint Res*. 2012;1(8):192-197. https://doi.org/10.1302/2046-3758.18.2000102
39. Forsberg JA, Pepek JM, Wagner S, et al. Heterotopic ossification in high-energy wartime extremity injuries: prevalence and risk factors. *J Bone Joint Surg Am*. 2009;91(5):1084-1091. https://doi.org/10.2106/JBJS.H.00792
40. Brown KV, Dharm-Datta S, Potter BK, et al. Comparison of development of heterotopic ossification in injured US and UK armed services personnel with combat-related amputations: preliminary findings and hypotheses regarding causality. *J Trauma*. 2010;69(Suppl 1):S116-S122. https://doi.org/10.1097/TA.0b013e3181e44cc7
41. Wosczyna MN, Biswas AA, Cogswell CA, et al. Multipotent progenitors resident in the skeletal muscle interstitium exhibit robust BMP-dependent osteogenic activity and mediate heterotopic ossification. *J Bone Miner Res*. 2012;27(5):1004-1017.
42. Huber AK, Patel N, Pagani CA, et al. Immobilization after injury alters extracellular matrix and stem cell fate. *J Clin Invest*. 2020;130(10):5444-5460. https://doi.org/10.1172/JCI136142
43. Xu J, Wang Y, Li Z, et al. PDGFRalpha reporter activity identifies periosteal progenitor cells critical for bone formation and fracture repair. *Bone Res*. 2022;10(1):7. https://doi.org/10.1038/s41413-021-00176-8
44. Molligan J, Mitchell R, Schon L, et al. Influence of bone and muscle injuries on the osteogenic potential of muscle progenitors: contribution of tissue environment to heterotopic ossification. *Stem Cells Transl Med*. 2016;5(6):745-753. https://doi.org/10.5966/sctm.2015-0082
45. Kan C, Chen L, Hu Y, et al. Gli1-labeled adult mesenchymal stem/progenitor cells and hedgehog signaling contribute to endochondral heterotopic ossification. *Bone*. 2018;109:71-79. https://doi.org/10.1016/j.bone.2017.06.014
46. Olmsted-Davis EA, Salisbury EA, Hoang D, et al. Progenitors in peripheral nerves launch heterotopic ossification. *Stem Cells Transl Med*. 2017;6(4):1109-1119. https://doi.org/10.1002/sctm.16-0347